Remarkable Affinity and Selectivity for Cs^+ and Uranyl (UO_2^{2+}) Binding to the Manganese Site of the Apo-Water Oxidation Complex of Photosystem II†

Gennady M. Ananyev, Andrew Murphy, Yuriko Abe,‡ and G. Charles Dismukes*

Department of Chemistry, H. Hoyt Laboratory, Princeton University, Princeton, New Jersey 08544

Received January 5, 1999; Revised Manuscript Received April 5, 1999

ABSTRACT: The size and charge density requirements for metal ion binding to the high-affinity Mn^{2+} site of the apo-water oxidizing complex (WOC) of spinach photosystem II (PSII) were studied by comparing the relative binding affinities of alkali metal cations, divalent metals (Mg^{2+}, Ca^{2+}, Mn^{2+}, Sr^{2+}), and the oxo-cation UO_2^{2+}. Cation binding to the apo-WOC-PSII protein was measured by: (1) inhibition of the rate and yield of photoactivation, the light-induced recovery of O_2 evolution by assembly of the functional $Mn_4Ca_1Cl_x$, core from its constituent inorganic cofactors (Mn^{2+}, Ca^{2+}, and Cl^-); and by (2) inhibition of the PSII-mediated light-induced electron transfer from Mn^{2+} to an electron acceptor (DCIP). Together, these methods enable discrimination between inhibition at the high- and low-affinity Mn^{2+} sites and the Ca^{2+} site of the apo-WOC-PSII. Unexpectedly strong binding of large alkali cations ($Cs^+ \gg Rb^+ > K^+ > Na^+ > Li^+$) was found to smoothly correlate with decreasing cation charge density, exhibiting one of the largest Cs^+/Li^+ selectivities (≥ 5000) for any known chelator. Both photoactivation and electron-transfer measurements at selected Mn^{2+} and Ca^{2+} concentrations reveal that Cs^+ binds to the high-affinity Mn^{2+} site with a slightly greater affinity (2−3-fold at pH 6.0) than Mn^{2+}, while binding about 10^4-fold more weakly to the Ca^{2+}-specific site required for reassembly of functional O_2 evolving centers. In contrast to Cs^+, divalent cations larger than Mn^{2+} bind considerably more weakly to the high-affinity Mn^{2+} site ($Mn^{2+} \gg Ca^{2+} > Sr^{2+}$). Their affinities correlate with the hydrolysis constant for formation of the metal hydroxide by hydrolysis of water: $Me^{2+}_{aq} \rightarrow [MeOH]^+_{aq} + H^+_{aq}$. Along with the strong stimulation of the rate of photoactivation by alkaline pH, these metal cation trends support the interpretation that $[MnOH]^+$ is the active species that forms upon binding of Mn^{2+}_{aq} to apo-WOC. Further support for this interpretation is found by the unusually strong inhibition of Mn^{2+} photooxidation by the linear uranyl cation (UO_2^{2+}). The intrinsic binding constant for $[MnOH]^+$ to apo-WOC was determined using a thermodynamic cycle to be $K = 4.0 \times 10^{15}$ M^{-1} (at pH 6.0), consistent with a high-affinity, preorganized, multidentate coordination site. We propose that the selectivity for binding $[MnOH]^+$, a linear low charge-density monocation, vs symmetrical Me^{2+} dications is functionally important for assembly of the WOC by enabling: (1) discrimination against higher charge density alkaline earth cations (Mg^{2+} and Ca^{2+}) and smaller alkali metal cations (Na^+ and K^+) that are present in considerably greater abundance in vivo, and thus would suppress photoactivation; and (2) higher affinity binding of the one Ca^{2+} ion or the remaining three Mn^{2+} ions via coordination to form μ-hydroxo-bridged intermediates, apo-WOC-$[Mn(\mu\text{-}OH)_2Mn]^{3+}$ or apo-WOC-$[Mn(\mu\text{-}OH)Ca]^{3+}$, during subsequent assembly steps of the native $Mn_4Ca_1Cl_x$ core. In contrast to more acidic Me^{2+} divalent ion inhibitors of the high-affinity Mn^{2+} site, like Ca^{2+} and Sr^{2+}, Cs^+ does not accelerate the decay of the first light-induced intermediate, IM_1, formed during photoactivation (attributed to apo-WOC-$[Mn(OH)_2]^+$). The inability of Cs^+ to promote decay of IM_1, despite having comparable affinity as Mn^{2+}, is consistent with its considerably weaker Lewis acidity, resulting in the reprotonation of IM_1 by water becoming the rate-limiting step for decay prior to displacement of Mn^{2+}. All four different lines of evidence provide a self-consistent picture indicating that the initial step in assembly of the WOC involves high-affinity binding of $[MnOH]^+$.

Photosynthetic water oxidation is catalyzed by a manganese metalloenzyme called the water oxidation complex (WOC).[1] It is a component of a multisubunit protein complex called photosystem II (PSII) that also contains a photochemical reaction center for light-driven charge separation (for reviews, see refs *1*−*6*). The active site of the WOC contains minimally a redox-active tyrosine (Y161 of D1 protein), a

† This work was supported by U.S. Department of Agriculture NRICGP Grant 96-35306-3433 and by Grant GM39932 from the National Institutes of General Medical Sciences.

* To whom correspondence should be addressed. Fax: (609)-258-1980. E-mail: dismukes@chemvax.princeton.edu.

‡ On leave from Department of Chemistry, Faculty of Science, Nara Women's University, Nara 630, Japan.

[1] Abbreviations: Chl, chlorophyll; DCBQ, 2,5-dichloro-*p*-benzoquinone; DCIP, 2,6-dichlorophenolindophenol; Me, metal ion; MES, 2-(*N*-morpholino)ethanesulfonic acid; PSII, photosystem II; TPDBA, *N*,*N*,*N*′,*N*′-tetrapropionato-1,3-bis(aminomethyl)benzene; WOC, water oxidizing complex; Y_{ss}, steady-state yield of oxygen evolution under pulsed light.

10.1021/bi990023u CCC: $18.00 © 1999 American Chemical Society
Published on Web 05/14/1999

Scheme 1: Kinetic Steps Observed in the Assembly of the WOC by Photoactivation[a]

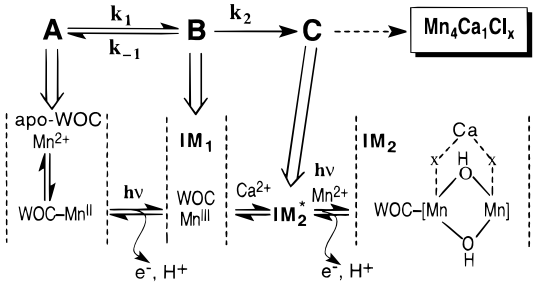

[a] The top part of the scheme presents a minimal kinetic model that fits the photoactivation data (*15*).

histidine residue (D1-H190), and an inorganic core comprised of three types of ions with a stoichiometry of $Mn_4Ca_1Cl_x$ that are all closely associated. The core can be assembled in a light-dependent process starting from the cofactor-depleted apo-WOC and simple inorganic salts containing all three essential cofactors. This process is called photoactivation and also occurs during biogenesis and normal PSII repair processing (*7, 8*).

Reassembly of active O_2-evolving WOC centers by photoactivation has been shown to require alternating light and dark steps (*8*), and also manganese, calcium, and chloride for full restoration of activity (*7*−*16*). Kinetic resolution of several steps has been achieved recently (*10*−*13, 15*), and some intermediates in the assembly process have been characterized by EPR spectroscopy (*13*−*14*). The kinetic data have been used to establish a minimal model given in Scheme 1 (*15*).

The first photolytic step, **A** ⇒ **B** involves an initial pre-steady-state lag phase in which one Mn^{2+} ion binds and is photooxidized to yield a Mn^{3+} ion. This step is coupled to release of a proton into solution, forming the first photolytic intermediate, IM_1, with a binding constant log $K_1^{-1} = 5.1$ (Table 1). This rapid photolytic step is followed by a slower dark kinetic phase that is rate-limiting, **B** ⇒ **C**, denoted $IM_1 \Rightarrow IM_2^*$ in Scheme 1. This dark step involves the binding of one Ca^{2+} ion and is presumed to involve slow folding of the protein to produce a new conformation that is capable of binding the remaining three Mn^{2+} ions with considerably higher affinity, thereby accounting for the cooperativity in Mn binding (*11*). Binding of the second Mn^{2+} ion and subsequent photooxidation convert IM_2^* to IM_2, a long-lived intermediate that can go on to bind two more Mn^{2+} ions and recover oxygen-evolving capacity in faster steps that have not been kinetically resolved. IM_2 is believed to be a spin-coupled dimanganese(III,III) pair based on EPR properties of a reduced precursor state (*14*).

A systematic study of the affinity and selectivity for inhibition of photoactivation by alternative inorganic cofactors is the subject of this paper. Such studies have not been possible until recently, due in part to inadequate sensitivity for O_2 concentration measurements and competition with photoinactivation of the apo-WOC protein (*10, 11*). Through a systematic examination of the binding affinities for various metal cations of known charge, ionic radius, free energy of solvation, and hydrolysis constant (Lewis acidity), one can assess what are the determinants of the binding affinities and thus infer the structural dimensions of the site and the energetics for cation binding and desolvation. Work has begun to examine these factors in the apo-WOC (*11, 12, 16*−*18, 19, 20*).

In the present article, we report the binding affinities of the alkali metal ions (Li^+, Na^+, K^+, Rb^+, and Cs^+) and selected divalent cations to the apo-WOC. Kinetic resolution of the first two steps in photoactivation is achieved using an ultrasensitive amperometric O_2 electrode which enables measuring the individual rate constants for assembly. We present quantitative measurements demonstrating unusually strong binding of Cs^+ and oxo-cations such as uranyl (UO_2^{2+}) specifically at the high-affinity Mn^{2+} site and comparatively weak binding to the Ca^{2+}-specific site required for assembly of the WOC. A self-consistent model for the initial steps of assembly of the WOC and cation inhibition is obtained.

MATERIALS AND METHODS

PSII-enriched membrane fragments were prepared from market spinach using Triton X-100 as a detergent (*21, 22*). Samples (at 1 mg of Chl/mL) were stored at −196 °C until they were slowly thawed and washed once in a medium containing 300 mM sucrose, 35 mM NaCl, 25 mM MES/NaOH buffer (pH 6.0), and 10% glycerol.

Manganese and calcium were removed (0.05−0.1 Mn/PSII) from PSII membrane fragments (0.25−1.0 mg of Chl/mL) using the assay medium [300 mM sucrose, 35 mM NaCl, 25 mM MES/NaOH buffer (pH 6.0)] along with 25−35 mM TPDBA [a bifunctional hydrophobic poly(aminocarboxylate) chelator, ($^-$**OOC**−CH_2−CH_2)$_2$=**N**−CH_2−C_6H_4−CH_2−**N**=(CH_2−CH_2−**COO**$^-$)$_2$] and 1 mM ascorbate, as described earlier (*10*−*12*).

Photoactivation of cofactor-depleted PSII membranes (apo-WOC) by light pulses (red LED's) and amperometric detection of dissolved O_2 in the assay medium containing 0.8 mM K_3FeCN_6 as electron acceptor were performed simultaneously in a home-built Clark-type microcell of 5 μL volume (*10, 11, 15*). A Pt/Ir electrode (4 mm in diameter) was covered with a thin silicone membrane capable of 100 ms time resolution. The current signal was amplified using a band-pass electronic filter between 0.03 and 10 Hz (Model 113, Hewlett-Packard). This filtering enables detection of the O_2 pulse produced by the LED flash (20−30 ms), while filtering the steady-state signal from dissolved O_2 in the sample. The amplified and filtered signal was digitized by a 12-bit data acquisition interface. Base line stripping was performed by digital subtraction to remove a minor flash artifact. The sensitivity for detection equals $\sim 5 \times 10^{-14}$ mol of O_2 per flash.

Electron transport was measured by photoreduction of DCIP (*17, 18*) using a diode array spectrophotometer (Model HP8452A, Hewlett-Packard) equipped with four ultra-bright LED's (maximum excitation at 660 nm) positioned at 45° to a 1 mm quartz cuvette.

The random error associated with measurements of the O_2 signal (Y_{ss}) or the initial electron transport rate was insignificant in comparison to the random variation between different samples. The estimated error in K_B, K_1, and K_m derived from these measurements performed on the same day on the same sample is equal to ±3%. The values of the kinetic constants measured on different samples can vary significantly, depending on the quality of biochemical preparations, on the age of the apo-PSII membranes, and on

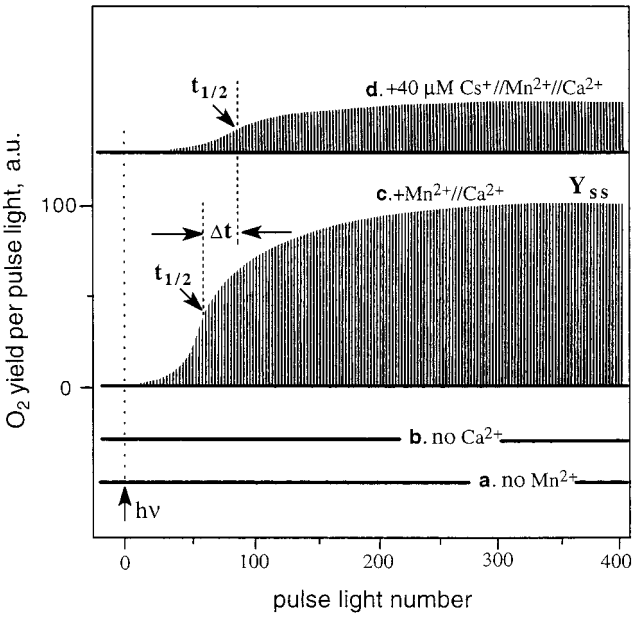

FIGURE 1: Typical kinetics of the rate of recovery of O_2 evolution by inorganic cofactors and inhibition by Cs^+. Each kinetic trace represents a sequence of 400 light pulses (LED with $t_{light} = 30$ ms and $t_{dark} = 3$ s) obtained with 100 ms time resolution. (a) To the assay medium were added all essential photoactivation constituents (1 μM apo-PSII/8 mM Ca^{2+}/0.8 mM K_3FeCN_6/43 mM Cl^-) except Mn^{2+}; (b) excluding only Ca^{2+}; (c) all photoactivation constituents are present including 8 μM Mn^{2+} and 8 mM Ca^{2+}; (d) effect of addition of 40 μM Cs^+ to conditions identical to the sample shown in panel C. The dark incubation of each sample before pulse illumination was 15 min. "a.u." in all figures refers to arbitrary units.

the amount and duration of exposure to the chelator used for extraction. By controlling these factors and using samples stored at −195 K for less than 3 months, the observed trends in the dependencies depicted on all plots were found not to vary from sample to sample. All derived quantities were determined at least twice under identical conditions.

All chemicals were analytical grade purity and purchased from Sigma or Aldrich. The purity of the CsCl (99.9%) was critical, and a stock solution was prepared directly before experimentation.

RESULTS

Inhibition by Alkali Metal Ions. Figure 1 (traces a−c) gives the time course for recovery of O_2 evolution by photoactivation of apo-WOC in the presence or absence of the standard inorganic constituents, including Ca^{2+}, Mn^{2+}, and Cl^-. The medium always contains 1 μM apo-WOC, saturating amounts of Cl^-, and an electron acceptor like K_3FeCN_6 or DCIP/DCBQ, as these are strictly necessary for assembly of the $Mn_4Ca_1Cl_x$ cluster. As previously reported, the kinetics are biphasic, with an initial lag phase followed by a single-exponential recovery of O_2 evolution. All centers undergo 99% reactivation based on previous comparison of the maximum yield (Y_{ss}) to the activity of an intact WOC that is depleted of the three extrinsic WOC polypeptides. The light pulses are of fixed duration (30 ms) and fixed dark interval (3 s). Trace d shows that 40 μM Cs^+ produces strong inhibition of the maximum yield of activated centers (Y_{ss}) and slows down the kinetics of assembly ($\Delta t_{1/2}$ increased by 30−60 s) versus a control without Cs^+. These effects contrast with the effect of Cs^+ on O_2 evolution in native (intact) PSII membranes (Figure 2, trace b), where 10 mM Cs^+ produces only a 6% decrease in the O_2 evolution rate of intact PSII membranes relative to the control (Figure 2, trace a). This result agrees with a previous study showing only a weak effect of Cs^+ on PSII membranes containing the intact $\{Mn_4\}$ cluster, but otherwise treated to remove Ca^{2+} ions and the three extrinsic polypeptides of the WOC (50% inhibition of Ca-reactivated O_2 evolution occurred at 10 mM Cs^+) (*23*). Thus, the strong binding (and inhibition) by Cs^+ to the apo-WOC protein complex occurs at a site which becomes exposed only following release of the $\{Mn_4\}$ cluster, since Cs^+ causes little inhibition of the intact WOC or the WOC lacking the three extrinsic polypeptides.

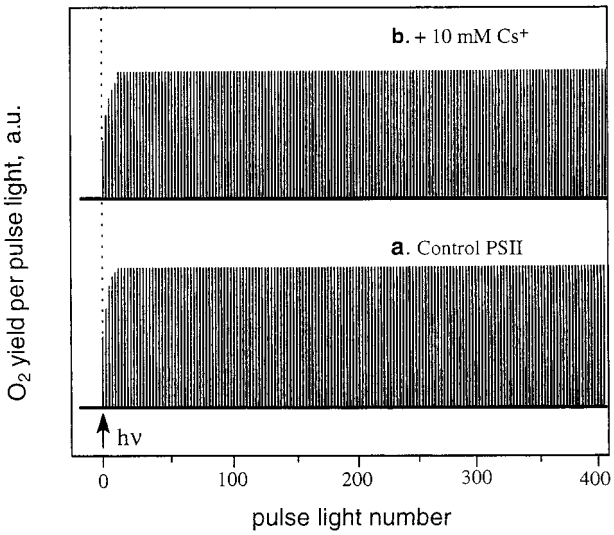

FIGURE 2: Kinetic traces demonstrating the effect of 10 mM Cs^+ on O_2 evolution by native PSII membranes with intact WOC. The same illumination conditions that are optimal for photoactivation are used here. Samples contain 1.6 mM $K_3Fe(CN)_6$ as an electron acceptor. Extraction of the 17, 23, and 33 kDa extrinsic WOC proteins by 1 M $CaCl_2$ washing does not increase the sensitivity of PSII membranes to Cs^+ inhibition.

Figure 3 compares the relative steady-state rate of O_2 evolution after completion of photoactivation (Y_{ss} proportional to the number of activatable apo-WOC centers) and the relative half-time for photoactivation vs the concentration of alkali metal salts (note the different concentration scales for Cs^+, Rb^+, and K^+). The overall binding constants (K_B) for inhibition of Y_{ss} are listed in Table 1 and plotted in Figure 4A, along with the results previously reported for NaCl, $MgCl_2$, and $CaCl_2$ (*10*, *12*, *15*). Figure 4A also shows that the K_B value for monovalent cations is opposite to that observed for divalent cations. Binding was studied in standard medium for supporting O_2 evolution (see Materials and Methods). K_B values are apparent binding constants, not equilibrium constants, since these measure a multistep nonequilibrium assembly process. Comparison of Figure 3 and Table 1 shows that both O_2 yield is inhibited and assembly half-time is retarded most efficiently by the larger alkali metal cations (Cs ≫ Rb > K > Na > Li), with a remarkably high affinity and selectivity for Cs^+. For the smaller cation K^+, a one-to-one correlation between O_2 yield and inverse of the assembly half-time (e.g., rate) could be followed over a wider range of concentrations and was found to be reciprocal, suggesting that the concentration of a single

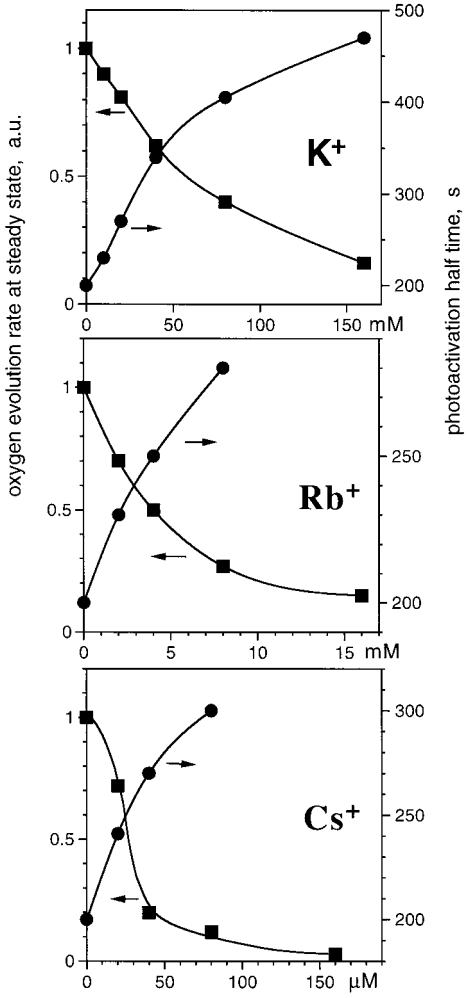

FIGURE 3: Effect of increasing concentration of the alkali metals (K^+, Rb^+, and Cs^+) on the recovery of O_2 evolution by photoactivation of spinach apo-WOC-PSII membranes. Both the yield of photoactivated centers after reaching a steady-state maximum, Y_{ss}, and the half-time, $t_{1/2}$, are shown. The alkali metal salts used are CsCl, RbCl, or KCl (note the different concentration scales for K^+, Rb^+, and Cs^+). The absolute yield of photoactivatable PSII centers is 100% of the initial population of active centers. Absolute half-times can vary from 110 to 200 s, increasing with sample history (aging). Rate constants were determined on at least three samples using methods previously described (*15*). Within a single data set, deviations were ≤2%. Cs^+ inhibition of photoactivation was found to be reversible by removal of Cs^+ by 2-fold washing in the dark with fresh assay medium. Other experimental conditions as in Figures 1 and 2.

pre-steady-state intermediate appears to be reduced. With Cs^+ the correlation appears not to be strictly one-to-one; saturation of the half-time is not seen, suggesting a more complicated behavior. Doubling the Mn^{2+} concentration from 8 to 16 μM/PSII revealed that the Cs^+ concentration required to inhibit Y_{ss} also increased by 2-fold, from 30 to 61 μM (Table 2). Taken together, the data suggest that alkali metal cations inhibit by displacing Mn^{2+} or Ca^{2+} or both ions at one or more steps during photoactivation.

Determination of the Individual Steps. To identify which step(s) during assembly at which Cs^+ might act, we resolved the time dependence of recovery of O_2 evolution into the initial steps noted in Scheme 1, using previously reported methods (*15*). A representative data set such as the control sample from Figure 1c is shown in the insert of Figure 5, replotted as the log of the fraction of inactive centers. This graphical format reveals two sequential steps: an initial lag phase followed by an exponential recovery of O_2 evolution.

Table 1: Apparent Binding Constants (K_B) for Metal Ion Inhibition of Photoactivation Yield (Recovery of O_2-Evolving Centers) in Spinach Apo-WOC-PSII[a]

ion	radius (Å)	K_B (M^{-1})	$1/K_1$ (M^{-1})	$K_{hydrolysis}$[d]
Sr^{2+}	1.13	4.3	360	6
Ca^{2+}	1.00	14	710	20
Mn^{2+}	0.80	22[b]	125000	2500
Mg^{2+}	0.66	45		380
Cs^+	1.67	33300	152000[c]	
Rb^+	1.47	250		
K^+	1.33	15		0.35
Na^+	0.97	1.25		0.63
Li^+	0.68	1.0		2.29
UO_2^{2+}	–	65400		1.58×10^8

[a] $1/K_1$ is the equilibrium binding constant for metal ion inhibition of Mn^{2+} binding to the initial (high-affinity) Mn^{2+} binding site (site **A** in Scheme 1), measured from the data for kinetics of photoactivation in Figure 5. The data were obtained at a Ca^{2+} concentration of 8 mM (except for the Ca inhibition data) and at pH 6.0. log plots are given in Figure 4A. [b] Excess Mn^{2+} inhibits photoactivation at high concentration while also being a required cofactor for photoactivation. [c] Values of $1/K_1 = 3.3 \times 10^5$ and 37 M^{-1} for Cs^+ binding to the high- and low-affinity Mn^{2+} sites, respectively, were also determined from the inhibition of the rate of photoreduction of DCIP by apo-WOC-PSII using Mn^{2+} as the electron donor. See text for details. [d] Data from ref *27*.

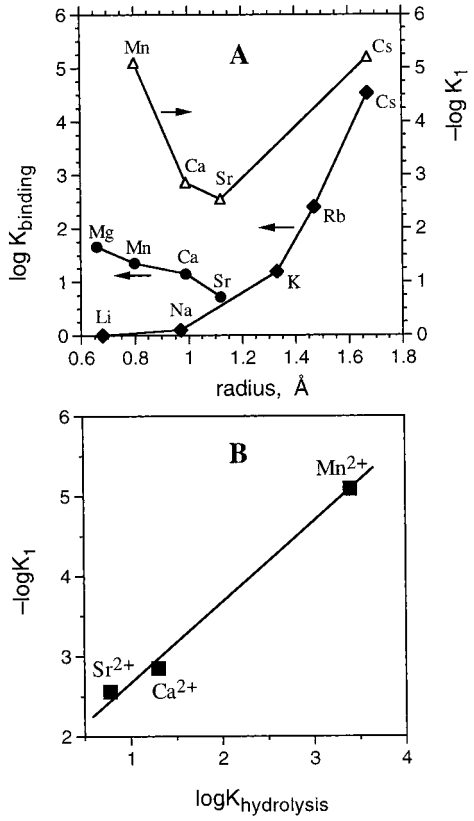

FIGURE 4: (A) Apparent inhibition constants (log K_B) for metal cation inhibition of photoactivation yield (Y_{ss}) vs ionic radii of the free cations. The alkali metal cations are plotted using diamonds (◆), while divalent cations are plotted with circles (●). The open triangles (△) for Mn^{2+}, Ca^{2+}, Sr^{2+}, and Cs^+ represent the true equilibrium binding constants at the high-affinity Mn^{2+} site determined from kinetics such as given in Figure 5: $-\log K_1 = -\log (k_1/k_{-1})$. (B) Metal ion binding affinity constant for apo-WOC ($-\log K_1$) versus the formation constant for the free metal hydroxide, $[MeOH]^+$, in solution ($K_{hydrolysis}$) (eq 1) (see text).

Table 2: Inhibitory Effect of Cs^+ and Sr^{2+} on Photoactivation Yield at Different Mn^{2+} and Ca^{2+} Concentrations[a]

ion	$[Mn^{2+}]$ (μM)	$[Ca^{2+}]$ (mM)	K_B (μM)
Cs^+	8	8	30
Cs^+	16	8	61
Cs^+	8	2	21.5
Cs^+	8	80	54
Sr^{2+}	8	0	230 mM

[a] K_B is the Michaelis constant for 50% inhibition of the yield of photoactivation, measured from the dependence of Y_{ss} on Cs^+ or Sr^{2+} concentration. The inhibition of Y_{ss} by Sr^{2+} was examined in the absence of Ca^{2+}, since Sr^{2+} exhibits an initial stimulatory region from 0 up to 40 mM Sr^{2+}, followed by the inhibitory region above 40 mM Sr^{2+}. Standard assay medium was used, and the apo-WOC concentration was 1 μM.

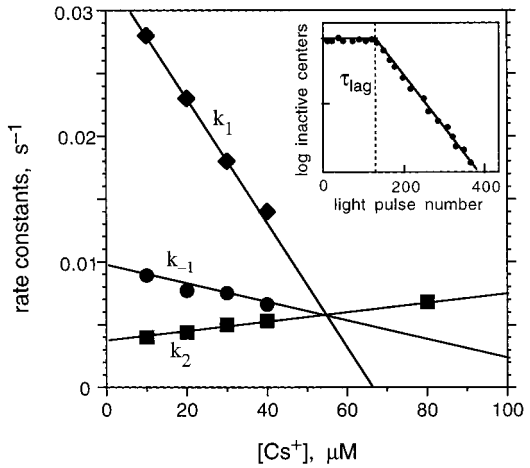

FIGURE 5: Rate constants k_1, k_{-1}, and k_2 for recovery of O_2-evolving activity by photoactivation in spinach apo-WOC-PSII vs the concentration of Cs^+. Refer to Scheme 1 for definitions. Conditions as in Figures 1 and 2 with 8 μM $MnCl_2$ and 8 mM $CaCl_2$ and 1 μM apo-WOC-PSII. The inset shows the semilogarithmic plot of the fraction of inactive centers versus pulse number calculated from Figure 1C.

These steps refer to formation of the first and second intermediates, IM_1 and IM_2*, respectively (Scheme 1).

Direct experimental determination of k_{-1}, the rate constant for decay of IM_1, was carried out by interruption of the usual pulse light illumination with a dark period of variable duration. The dark period was started after 0−70 s of pulse light illumination at the end of the lag phase, as determined by linear extrapolation of plots of log (fraction inactive centers) vs time obtained from the data analogous to those in Figure 5 (inset). The half-time required for recovery of the original lag period was taken as the half-life time for decay of IM_1 in the dark. The rate constant for the rate-determining step of photoactivation, k_2, was obtained from the negative slope of the semilogarithmic plot of the fraction of the inactive centers vs time in the interval starting immediately after the break point and followed for at least 80−90% recovery, Figure 5 (inset). Determination of k_1 was calculated in a self-consistent way using the values of k_{-1} and k_2 and the two-step kinetic model (Scheme 1). Specifically, we adopted the assumption that the end of the lag phase corresponds to the time when the concentration of IM_1 reaches its maximum, so that preequilibrium is established with k_1, $k_{-1} > k_2$. This assumption was verified by the observation that the second step always obeyed a single-exponential recovery of activity over >90% of the population.

The resulting dependencies of the pseudo-first-order rate constants k_1, k_{-1}, and k_2 (defined in Scheme 1) on Cs^+ concentration are plotted in Figure 5 for standard photoactivation conditions (8 μM $MnCl_2$, 8 mM $CaCl_2$, and 1 μM apo-WOC). The data show that Cs^+ exerts its strongest inhibitory effect by suppressing k_1, the binding and photooxidation of the initial Mn^{2+}. A 2-fold reduction is seen between 10 and 40 μM CsCl concentration. The true equilibrium binding constant (K_1) for Cs^+ inhibition at this site (site **A** in Scheme 1), called the high-affinity Mn^{2+} site, can be obtained from a standard expression for inhibition kinetics (*24*):

$$[CS]_{50\%} = \left\{1 + \frac{[Mn]}{K_{Mn}}\right\}K_1$$

$$K_{Mn} = \frac{k_{-1}}{k_1}[Mn]$$

In this expression $[Cs]_{50\%}$ is the concentration of Cs^+ that causes 50% inhibition of the rate of step 1, while K_{Mn} is the dissociation constant for Mn^{2+} at this site. K_{Mn} was determined to be 8 μM in earlier measurements (*15*). Hence, the value of K_1 obtained from the data in Figure 5 is 6 μM at pH 6, a slightly higher affinity for Cs^+ than for Mn^{2+}. The Cs^+ affinity at the high-affinity Mn^{2+} site is about 5 times greater than its net affinity overall for inhibition of the yield of activatable centers (K_B in Figure 3 and Table 1). The somewhat weaker concentration dependence for inhibition of the yield of activatable centers has two origins. The yield depends on all three rate constants. As seen in Figure 5, Cs^+ not only inhibits by blocking the binding of Mn^{2+} in the first step, but also weakly stimulates k_2, thereby accelerating the rate-limiting dark conformational step ($IM_1 \Rightarrow IM_2$*) which Ca^{2+} induces in the native system. There is a 20% increase in k_2 between 10 and 40 μM Cs^+ that is offset by an equally small reduction in the rate of the back reaction k_{-1}, slowing the decay of the first intermediate ($IM_1 \Rightarrow$ apo-WOC + Mn^{2+}). The latter result was unexpected since Cs^+ rebinding to the high-affinity Mn^{2+} site restores the initial dark state and thus should displace Mn^{2+} and hence accelerate k_{-1}. By contrast, divalent cations which bind more weakly to the high-affinity Mn^{2+} site, like Ca^{2+} and Sr^{2+}, accelerate the decay of IM_1 by displacing Mn^{2+} in a process that is unimolecular in Ca^{2+} concentration (*15*). The absence of an appreciable dependence of k_{-1} on the concentration of Cs^+ in Figure 5 indicates that the rate of decay of IM_1 is not controlled by the rate at which Cs^+ displaces Mn^{2+}, but rather by a preceding step that is independent of Cs^+ concentration. Although the nature of this rate-limiting step remains unresolved, there are two leading candidates: either the rate of reduction of Mn^{3+} to Mn^{2+}, or the rate of reprotonation of IM_1 [a proton is released in the light upon forming IM_1 (*12*)]. These possibilities are shown in Scheme 2, where the formation of IM_1 is proposed to proceed in two steps: initial binding of Mn^{2+}_{aq} in competition with Cs^+ to form $[MnOH]^+$-WOC with transfer of a proton to an endogenous base (B), followed by photooxidation to form IM_1.

The experiment reported in Figure 3 was repeated at different concentrations of Ca^{2+} in the medium in order to

Scheme 2: Proposed Intermediates and Mechanism of Cs^+ Interaction with Apo-WOC[a]

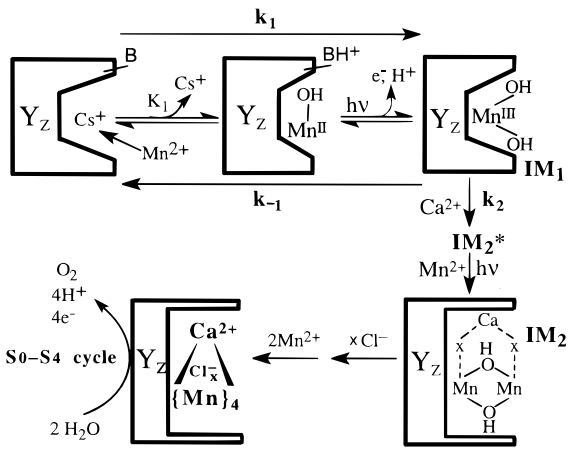

[a] An intrinsic base (B) is omitted for clarity after the first step.

learn if the Cs^+ binding affinity depends on either the presence of Ca^{2+} in the medium or the Ca-induced conformational change of the apo-WOC. We found only a weak competition between Ca^{2+} and Cs^+, about a 2-fold increase in the amount of Cs^+ required to cause 50% inhibition of the photoactivation yield (Y_{ss}) between 2 and 80 mM Ca^{2+} (see K_B value in Table 2). These experiments show that the conformational change of the WOC produced by the binding of Ca^{2+} in step k_2 plays essentially no role in the binding of Cs^+. This result further supports the conclusion reached above that Cs^+ binds to the high-affinity Mn^{2+} site in the apo-WOC protein, since this site (**A**) is known to bind ions essentially independent of the Ca-induced conformational change (step **B** ⟹ **C**, Scheme 1).

Comparison of K_B and K_1 for Divalent versus Monovalent Cations. A plot of the logarithm of the apparent binding constant for inhibition of O_2 yield, log K_B, vs the metal ionic radius (*25*) is given in Figure 4A. This plot reveals that a strong correlation exists between increasing ionic radius of the alkali cations and increasing binding affinity. The lowest affinity is found for the smallest monocation Li^+ (0.68 Å), while the largest affinity is found for Cs^+ (1.67 Å; more than 5000-fold greater affinity). Separate correlation curves are drawn for the alkali metal monocations (Cs, Rb, K, Na, Li) and for the divalent cations studied (Sr, Ca, Mn, Mg). The dications exhibit a weaker trend opposite to the monocations, with the larger Sr^{2+} ion binding the weakest of the three (Table 1). Although Mn^{2+} is required for photoactivation, excess Mn^{2+} nonspecifically inhibits O_2 evolution like many other cations (*10*, *16*, *26*). Thus, in Figure 4A we report the inhibition of photoactivation yield (K_B) by excess Mn^{2+}.

K_B is not a true equilibrium binding constant since it measures the net affinity for inhibition of photoactivation and so may reflect multiple binding sites. Hence, in Figure 4A we also compare the kinetically derived equilibrium binding constants, plotted as log($1/K_1$), for binding to the high-affinity Mn^{2+} site by Mn^{2+}(activation) and by Ca^{2+}, Sr^{2+}, and Cs^+ (all inhibitors). These data indicate that Mn^{2+} binds 170 times stronger than Ca^{2+} and 3400 times stronger than Sr^{2+}, and that a minimum occurs for cation affinity at a radius intermediate between Cs^+ (1.67 Å) and Sr^{2+}(1.13 Å).

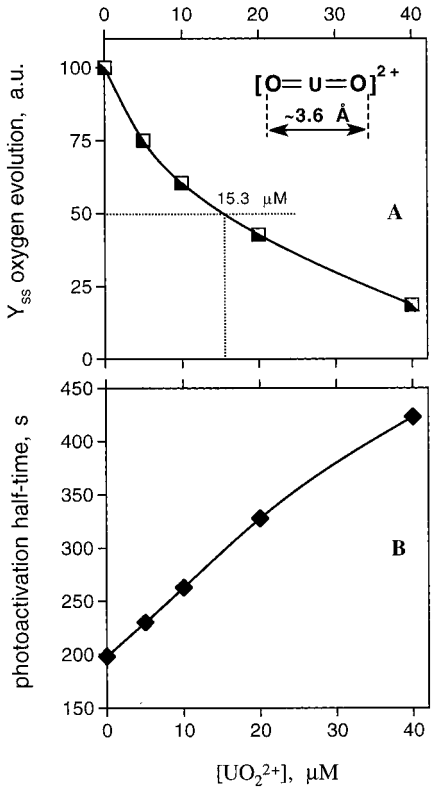

FIGURE 6: (A) Inhibition by the uranyl cation, UO_2^{2+}, of photoactivation yield in spinach apo-WOC-PSII at steady-state (Y_{ss}) and (B) half-time. Experimental conditions as in Figures 1 and 2.

Taken together the affinity data for mono- and divalent cations (Table 1 and Figure 4A) reveal the following: (1) there are opposite trends for binding these metal ions; larger monovalent cations bind with increasing affinity, while divalent ions larger than Mn^{2+} bind with decreasing affinity; (2) there is a surprisingly large affinity for Cs^+ comparable to that for Mn^{2+}; (3) small divalent cations bind more strongly than monocations of comparable radius (Ca^{2+} and Sr^{2+} vs Na^+ and K^+); (4) binding affinities for the divalent cations to apo-WOC correlate with the binding constants for formation of the metal hydroxides (Table 1 and eq 1):

$$Me^{2+} + OH^- \Longrightarrow [MeOH]^+ \qquad (1)$$

This correlation is plotted in Figure 4B for the three divalent cations for which quantitative measurements of K_1 were made ($[MnOH]^+$, $[CaOH]^+$, and $[SrOH]^+$) Although only three examples have been measured, the values for K_1 and $K_{hydrolysis}$ show a positive linear correlation over a considerable range of 3 orders of magnitude. Because larger rather than smaller alkali cations inhibit most effectively, and binding affinities for divalent cations correlate with $K_{hydrolysis}$, we propose that the initial species that binds to apo-WOC is likely $[MnOH]^+$.

Effect of Uranyl, UO_2^{2+}, on Y_{ss} and $t_{1/2}$. To test this idea further, we investigated inhibition by the stable oxo-cation uranyl, UO_2^{2+}. The results given in Figure 6A,B reveal that uranyl causes strong inhibition of the yield and increases the half-time for photoactivation with a dissociation constant of $K_B = 15.3$ μM. Therefore, uranyl must bind to a high-affinity site located at or before the rate-limiting step. This observation could be consistent with the blocking by UO_2^{2+} of the first or second step in photoactivation in Scheme 1.

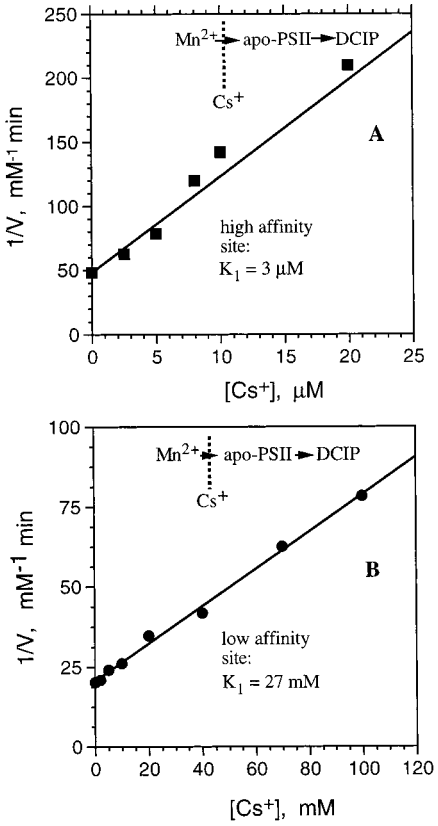

FIGURE 7: Dixon plot of the inverse of the initial rate of DCIP photoreduction by apo-WOC-PSII in the presence of exogenous Mn^{2+} as electron donor, plotted as a function of the concentration of added CsCl. Rate measurements were made spectrophotometrically in the standard photoactivation assay medium, except with Mn^{2+} concentrations o: (A) 5 μM and (B) 100 mM. The derived inhibition constants for Cs^+ at these Mn^{2+} concentrations are given in the figure and were obtained from analysis of the Dixon plots using the affinity constants for Mn^{2+} at the high- and low-affinity sites (5 and 300 μM, respectively) (*17*). All samples contain 0.2 μM apo-WOC-PSII and 100 μM DCIP as electron acceptor. Samples were incubated in the dark for 5 min before measurements.

Alternatively, UO_2^{2+} may accelerate the decay of IM_1 (k_{-1}) which would produce the same effect on yield and half-time. The behavior of UO_2^{2+} is very similar to the behavior of Cs^+ in Figure 3 (bottom panel).

Cs^+ Blocks Mn^{2+}-Dependent Electron Transport in Apo-WOC. The photoactivation data in Figures 3−5 and Tables 1 and 2 suggest that Cs^+ competes for binding to the high-affinity Mn^{2+} site, site **A** (Scheme 1). To more completely test this conclusion, we examined the ability of Cs^+ to inhibit the light-induced electron donation by exogenous Mn^{2+} to apo-WOC, using DCIP as a terminal electron acceptor: Mn^{2+}⟹apo-WOC⟹DCIP. This method enables a direct assay of Mn^{2+} electron donation at both the high- and low-affinity Mn^{2+} sites (*17*). The time dependence of the light-induced optical absorbance change from DCIP was monitored as a function of Cs^+ concentration in the absence of Ca^{2+}. The initial rates extrapolated to zero time are plotted in Figure 7A,B in the form of reciprocal velocity vs Cs^+ concentration, so-called Dixon plot analysis (*24*). Kinetic evidence for competition between Cs^+ and Mn^{2+} binding was established over a wide range of Cs^+ concentrations from analysis of such plots (data to be published). Representative raw data (absorbance vs time) are given as Supporting Information (Figures S1 and S2). The plots show that Cs^+ inhibits Mn^{2+} photooxidation by apo-WOC at both high- and low-affinity sites with inhibition constants of $K_1^H = 3$ μM and $K_1^L = 27$ mM, respectively, at Mn^{2+} concentrations of 5 and 100 μM, respectively. The intrinsic inhibition constant for Cs^+ binding to the high-affinity site was determined from these measurements to be $1/K_1 = 3.5 \times 10^5$ M^{-1} (in the absence of Ca^{2+}). This value differs by only a factor of 2 from the measured inhibition constant for Cs^+ inhibition of photoactivation yield (Table 1). The intrinsic binding constants for Mn^{2+} at the high- and low-affinity sites that are needed for this calculation were measured to be 5 and 300 μM, respectively, values very close to those reported by Ghirardi et al. (*17*) using the same method.

We observed evidence that an unstable intermediate photoaccumulates during these measurements which exhibits a lower DCIP photoreduction rate, by examining the effect of a subsequent dark incubation period prior to re-illumination. In the case of the low-affinity site, no further DCIP photoreduction occurred, since almost all of the Mn^{2+} in the medium (5 μM) was consumed by the original illumination (Figure S1). By contrast, the low-affinity site regained the original rate of DCIP photoreduction after incubation for a few seconds in the dark. The latter sample has 500 μM Mn^{2+} which may accelerate the decay of the photoaccumulated intermediate by restoring the original apo-WOC-PSII center. The lifetime of this intermediate is extended by addition of Ca^{2+} and leads to productive photoactivation of O_2 evolution (*10, 26*). Hence, the kinetics for the decrease in the DCIP photoreduction rate appear to coincide with the kinetics for formation of IM_1 under comparable conditions, although no quantitative kinetic comparisons were made.

We also examined whether Cs^+ could inhibit light-induced electron donation to apo-WOC-PSII by the highly efficient reaction with diphenyl carbazide (*17, 18*): DPC ⟹ apo-WOC-PSII ⟹ DCIP. DPC donates an electron directly to the special redox-active tyrosine-161 (Y_Z) of the D1 protein and only weakly interacts with the high-affinity Mn^{2+} site (*17*). We observed less than 2% inhibition of this reaction by 0.5 mM Cs^+, a concentration that completely inhibits electron donation from Mn^{2+} and photoactivation. Therefore, inhibition of the latter two reactions by Cs^+ must involve inhibition of binding of Mn^{2+} to apo-WOC, since electron donation directly to Y_Z^+ by DPC is not affected.

Taken altogether, the photoactivation and electron donation data form a self-consistent picture demonstrating that Cs^+ blocks electron donation by Mn^{2+} at two sites in apo-WOC. Also, since Ca^{2+} is not present in the electron donation assay, inhibition by Cs^+ of Mn^{2+} photooxidation occurs before the calcium-induced conformational change at IM_2 (Scheme 1).

It is interesting to speculate whether the low-affinity Mn^{2+} site probed by Cs^+ inhibition of electron transport (Figure 7A,B) may actually be equivalent to the intrinsic calcium site required for assembly of the $\{Mn_4\}$ core. This hypothesis could be tested by examination of the Ca^{2+} concentration dependence for inhibition of Mn^{2+}-dependent photooxidation. If true, this evidence would place the Ca^{2+} site within close range to both the high-affinity Mn^{2+} site and Y_Z, a conclusion that has already been suggested by EPR results demonstrating the formation of a calcium-induced, spin-coupled Mn_2(II,II) site during photoactivation (*14*).

DISCUSSION

The strong inhibition of the yield of photoactivated centers by Cs^+ (Figures 3−5) and by the metal-oxo cation UO_2^{2+} (Figure 6) occurs at a site which becomes exposed only following release of the tetramanganese cluster, since Cs^+ (and UO_2^{2+}) causes very little inhibition of the intact WOC (Figure 2). The agreement of the measured inhibition constant for Cs^+ inhibition of photoactivation (6 μM dissociation constant) and Mn^{2+} electron donation (3 μM), given in Table 1, reveals that Cs^+ binds to the high-affinity Mn^{2+} site of apo-WOC.

The proposed mechanism for inhibition by Cs^+ and other ions at the high affinity site (Scheme 2) may appear not to explain the inhibition of recovery of the steady-state O_2 yield based on the expectation that photoactivation of the uninhibited apo-WOC is an irreversible process that leads to a stable WOC with 100% recovery of activity. However, photoactivated apo-WOC centers are lacking the three extrinsic polypeptides (17, 23, and 33 kDa WOC proteins) and possibly other smaller subunits essential for in vivo stability, and thus are not indefinitely stable to disassembly by reducing agents (reduced electron acceptors) or high concentrations of ions, unlike the intact WOC complex. Cs^+ may also inhibit steps following the rate-limiting step of assembly that are not detected with the present method, and thus not included in Scheme 2.

The affinity data in Figure 4A are intriguing. Why does the affinity for the alkali metal cations increase as size increases, even exceeding the Mn^{2+} affinity in the case of Cs^+? We believe that this is a true manifestation of the actual size preference for cation binding to the high-affinity Mn^{2+} site, which is designed to bind an oxo-manganese cluster of uncertain structure. We propose that Cs^+ binds strongest to the high-affinity Mn^{2+} site because its charge density (ion radius 1.67 Å) matches better than any other cation found to date at this site. Such a high affinity for Cs^+ would make sense if the high-affinity Mn^{2+} site is optimized for binding the hydrolysis product $[MnOH]^+$ rather than the aqua dication Mn^{2+}_{aq} (ion radius 0.80 Å). $[MnOH]^+$ has the same charge as Cs^+ and comparable size, although distributed in the form of a dipolar triatomic species. This interpretation also provides a reasonable explanation for why Cs^+ does not appreciably accelerate the decay of IM_1 (Figure 5), since rebinding of a proton should then become rate-limiting for decay of IM_1 to form apo-WOC and Mn^{2+}_{aq} (Scheme 3). By contrast, more acidic dications such as Ca^{2+} actually induce decay of IM_1. The unimolecular rate constant for decay of IM_1 (k_{-1} in Scheme 1) exhibits a first-order dependence on the calcium concentration (*15*), and is 4-fold slower if the weaker Lewis acid Sr^{2+} replaces Ca^{2+} (Zaltsman, Ananyev, and Dismukes, unpublished results). These kinetic data suggest a Lewis acid role for the alkaline earth ions to reprotonate $[MnOH]^+$ upon displacement of Mn^{2+} by Ca^{2+}. This proposal is also consistent with the pH dependence of photoactivation yield and kinetics which exhibit strong alkaline activation, previously ascribed to the release of a proton prior to the rate-limiting step (*10*).

How could WOC-$[MnOH]^+$ form in sufficient amount to account for photoactivation? The equilibrium constant for spontaneous formation of free $[MnOH]^+$ by hydrolysis of water is very small, 3.2×10^{-11} ($pK_a = 10.5$); hence, there would not be much present free in solution at the acidic−neutral pH commonly found in the lumenal space of thylakoids. However, formation of WOC-$[MnOH]^+$ at the high-affinity site of apo-WOC could be driven by two factors: first, if there exists a basic residue that can serve as proton acceptor during hydrolysis of Mn^{2+}; and, second, if the intrinsic binding affinity for $[MnOH]^+$ is greater than that for Mn^{2+}. The intrinsic binding constant for binding of $[MnOH]^+$ to apo-WOC, independent of the dark proton ionization step of Mn^{2+}_{aq}, can be calculated from the thermodynamic cycle given in the lower part of Scheme 3. This calculation utilizes the known pK_a of Mn^{2+}_{aq}, and yields a value of 4.0×10^{15} M^{-1}. Such a large affinity indicates that the binding site for $[MnOH]^+$ to apo-WOC is typical of a preorganized polydentate chelate complex with multiple donor atoms participating in coordination (*27*).

Scheme 3: Energetics of Mn^{2+} Binding to the High-Affinity Mn^{2+} Binding Site and H^+ Release during Assembly of the WOC by Photoactivation

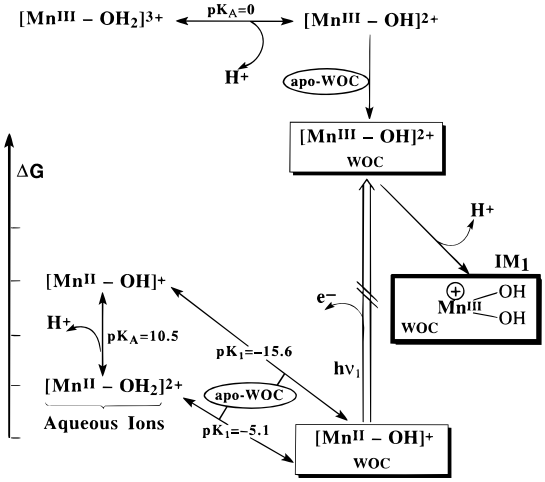

Also depicted in the upper part of Scheme 3 is a hypothetical thermodynamic pathway involving hydrolysis of Mn^{3+}_{aq} to form $[MnOH]^{2+}$, followed by binding to apo-WOC to form the same transient intermediate that is produced prior to IM_1 during photoactivation. This pathway has not been observed owing to the extreme oxidative reactivity of uncomplexed Mn^{3+}_{aq}. The idea summarized in Scheme 3, that WOC-$[MnOH]^+$ is the dark precursor required for subsequent photoassembly intermediates, is also supported by studies demonstrating strong binding by other metal-oxo cations such as UO_2^{2+} to the high-affinity Mn^{2+} site (Figure 6). The uranyl cation is linear with an O−O distance of 3.6 Å.

Further evidence supporting $[MnOH]^+$ as an early intermediate in formation of the WOC comes from several sources. The intact $Mn_4Ca_1Cl_x$ cluster of the WOC is believed to contain oxo-bridges between Mn^{3+} and Mn^{4+} ions based on Mn EXAFS studies (*6*), and these presumably form by hydrolysis of water ligands during assembly. The pH dependence of photoactivation reveals that alkaline conditions greatly stimulate the rate of assembly; between pH 5.4 and 6.8 the rate increases linearly by 3-fold (*10*). Studies of the dependence on the buffer capacity also show that a proton is released following illumination upon formation of IM_1 (*11*). Preliminary results using a H^+-sensitive field effect transistor to monitor proton evolution also support this result

(Ananyev, Mincer, and Dismukes, unpublished results). Last, $[MnOH]^+$ has been implicated as an intermediate in the formation of high-valent multinuclear Mn−oxo complexes (*28*, *29*).

The minimum in cation affinity between Cs^+ and Sr^{2+} in Figure 4A suggests the possibility that natural selection during biological evolution may have purposely designed the high-affinity Mn^{2+} site so that its affinity for abundant physiologically important cations such as Na^+, K^+, Mg^{2+}, and Ca^{2+} would be minimized relative to Mn^{2+}. These physiologically widespread cations are found in considerably greater abundance in plants relative to Mn^{2+}, a trace metal, and would therefore effectively inhibit assembly of the WOC if not discriminated against. Discrimination by compartmentation or by binding site selectivity are conceivable methods. We conclude that the sizes of Na^+ and K^+ are too small and their charge distributions too symmetrical to permit them to be effective inhibitors of apo-WOC in competition with $[MnOH]^+$. Ca^{2+} is also a relatively poor inhibitor of the high-affinity Mn^{2+} site, about 200-fold weaker affinity than Mn^{2+} (Table 1). Free in solution, it is also a weaker Lewis acid by about 100-fold vs Mn^{2+} and thus will be correspondingly less capable of inducing proton ionization that is needed for forming $[CaOH]^+$, the proposed inhibitory species. Mg^{2+} is reported to be a weaker Lewis acid than Mn^{2+}, and should therefore also be less capable of ionization to form $[MgOH]^+$ (*27*). It would be useful to measure the effect of Mg^{2+} on K_1 to see if it too correlates with hydrolysis to $[MgOH]^+$. However, the speciation of Mg^{2+}_{aq} into aggregates would need to be accounted for (*27*).

The size preference for larger alkali cations at the high-affinity Mn^{2+} site appears to be a consequence of nature purposely designing the site to stabilize formation of Mn−hydroxo and eventually Mn−oxo complexes, that could serve as the bridging site to the next Mn^{2+} ion and possibly the Ca^{2+} ion during assembly of the $Mn_4Ca_1Cl_x$ core of the WOC (Scheme 2). The cooperative uptake of 4.0 Mn^{2+} ions per apo-WOC during photoactivation indicates that the affinity of the second and subsequent Mn^{2+} ions increases relative to the preceding ones. This increased affinity could be explained by formation of μ-oxo or μ-hydroxo bridges between oxidized Mn ions, and by protein conformational changes which increase Mn^{2+} binding affinity during assembly.

Scheme 2 also provides a summary of the proposed structure of the second light-induced intermediate IM_2 (*13*, *14*). This intermediate is known to contain two Mn^{3+} ions and one Ca^{2+} based on the molecularity of the individual photoactivation steps (*15*). IM_2 is believed to form a spin-coupled ligand-bridged dimanganese(III,III) complex based on EPR evidence showing that it can be formed from a spin-coupled dimanganese(II,II) precursor known to bind in the dark to the apo-WOC protein following calcium-induced folding (*14*). Calcium plays a crucial role in the binding of the second Mn(II) ion and expression of inter-manganese dipolar coupling, since only mononuclear (i.e., spin-uncoupled) Mn(II) EPR signals could be detected in the absence of calcium. On the basis of the data given herein and elsewhere (*14*), we propose that the ligands that serve to provide the spin-coupling interaction between the Mn(III) ions in IM_2 are likely to be deprotonated water ligands, in the form of μ-hydroxo or μ-oxo ions.

Finally, it is significant that Cs^+ binds more strongly than K^+, Na^+, and Li^+ by factors of 2000, 2700, and 5000, respectively (Table 1), indicating a higher selectivity for the larger alkali metal cations than has been achieved with any synthetic or biological chelator (*30*, *31*). This high selectivity suggests that apo-WOC-PSII may prove useful as a scavenger of man-made radionuclides (^{134}Cs and ^{137}Cs) found as environmental pollutants (for reviews, see ref *32*), or for separation of radioactive ^{134}Cs and ^{137}Cs produced in nuclear fuels from fission reactors, where discrimination against a high background of Na^+ and K^+ is essential (*33*, *34*). Nature's design of the high-affinity Mn^{2+} binding site of apo-WOC-PSII could serve as a prototype for synthesis of new Cs^+-specific chelators.

In preliminary independent experiments it has been found that Cs^+ binding to apo-WOC-PSII in competition with Mn^{2+} can also be observed by detection of binding of radioactive $^{137}Cs^+$ (preliminary results obtained by J. Mincer, K. Nash, and M. Jensen in Argonne National Laboratory).

ACKNOWLEDGMENT

We thank Drs. M. Seibert, M. Ghirardi, M. Thurnauer, and R. K. Watt for helpful advice and J. S. Mincer for preliminary data on proton release and $^{137}Cs^+$ binding to apo-WOC-PSII.

SUPPORTING INFORMATION AVAILABLE

Figures showing Cs^+ inhibition of Mn^{2+} photooxidation by apo-WOC at both high- and low-affinity sites (5 pages). This material is available free of charge via the Internet at http://pubs.acs.org.

REFERENCES

1. Hankamer, B., Barber, J., and Boekema, E. J. (1997) *Annu. Rev. Plant Mol. Biol. 48*, 641−671.
2. Debus, R. J. (1992) *Biochim. Biophys. Acta 1102*, 269−352.
3. Britt, R. D. (1996) in *Oxygenic Photosynthesis: The Light Reactions* (Ort, D. R., and Yocum, C. F., Eds.) pp 137−164, Kluwer Academic Publishers, Dordrecht, The Netherlands.
4. Renger, G. (1993) *Photosynth. Res. 38*, 229−247.
5. Yachandra, V. K., Sauer, K., and Klein, M. P. (1996) *Chem. Rev. 96*, 2927−2950.
6. Riggs-Gelasco, P. J., Mei, R., Yocum, C. F., and Penner-Hahn, J. E. (1996) *J. Am. Chem. Soc. 118*, 2387−2399.
7. Cheniae, G. M., and Martin, I. F. (1971) *Biochim. Biophys. Acta 253*, 167−178.
8. Tamura, N., and Cheniae, G. M. (1987) *Biochim. Biophys. Acta 890*, 179−194.
9. Inoue, Y., Kobayashi, Y., Sakamoto, E., and Shibata, K. (1974) *Physiol. Plant 32*, 288−298.
10. Ananyev, G. M., and Dismukes, G. C. (1996) *Biochemistry 35*, 14608−14617.
11. Ananyev, G. M., and Dismukes, G. C. (1996) *Biochemistry 35*, 4102−4109.
12. Ananyev, G. M., Zaltsman, L., McInturff, R. A., and Dismukes, G. C. (1998) in *The Proceeding of the XI Photosynthesis Congress* (Garab, G., Ed.) Budapest, August 17−22, 1998, Hungary; Kluwer Academic Publishers, Dordrecht, The Netherlands (in print).
13. Ananyev, G. M., and Dismukes, G. C. (1995) in *Photosynthesis: From Light to Biosphere* (Mathis P., Ed.) Vol. II, pp 431−435, Kluwer Academic Publishers, Dordrecht, The Netherlands.
14. Ananyev, G. M., and Dismukes, G. C. (1997) *Biochemistry 36*, 11342−11350.

15. Zaltsman, L., Ananyev, G. M., Bruntrager, E., and Dismukes, G. C. (1997) *Biochemistry 36*, 8914−8922.
16. Miller, A.-F., and Brudvig, G. W. (1989) *Biochemistry 28*, 8181−8190.
17. Ghirardi, M. L., Lutton T. W., and Seibert, M. (1996) *Biochemistry 35*, 1820−1828.
18. Hsu, B.-D., Lee, J. Y., and Pan, R.-L. (1987) *Biochim. Biophys. Acta 890*, 89−96.
19. Ghirardi, M. L., Lutton, W. L., and Seibert, M. (1998) *Biochemistry 37*, 13559−13566.
20. Ghirardi, M. L., Preston, C., and Seibert, M. (1998) *Biochemistry 37*, 13567−13574.
21. Berthold, D. A., Babcock, G. T., and Yocum, C. F. (1981) *FEBS Lett. 134*, 231−234.
22. Ghanotakis, D. F., Babcock, G. T., and Yocum, C. F. (1984) *Biochim. Biophys. Acta 765*, 388−398.
23. Yocum, C. F. (1991) *Biochim. Biophys. Acta 1059*, 1−15.
24. Segel, I. H. (1975) *Enzyme Kinetics*, John Wiley & Sons, New York/Chichester/Brisbane/Toronto.
25. Weast, R., and Astle, M. J., Eds. (1982) in *CRC Handbook of Chemistry and Physics* (1982) 63rd ed., p F-179, CRC Press Inc., Boca Raton, FL.
26. Chen, C., Kazimir, J., and Cheniae, G. M. (1995) *Biochemistry 34*, 13511−13526.
27. Smith, R. M., and Martell, A. E. (1986) *Critical Stability Constants*, Vol. 4, Plenum Press, New York and London.
28. Reddy, K. R., Rajasekharan, M. V., Arulsamy, N., and Hodgson, D. J. (1996) *Inorg. Chem. 35*, 2283−2286.
29. Heyword, M. P., and Wells, C. F. (1987) *Transition Met. Chem. 12*, 179−181.
30. Izatt, R. M., Bradshaw, J. S., Bruening, R. L., Tarbet, B. J., and Bruening, M. L. (1995) *Pure Appl. Chem. 67*, 1069−1074.
31. Davis, J. T., Tirumala, S. K., and Marlow, A. L. (1997) *J. Am. Chem. Soc. 119*, 5271−5272.
32. Eisenbud, M. (1987) *Environmental Radioactivity*, Academic Press, London.
33. Schulz, W. W., and Bray, L. A. (1987) *Sep. Sci. Technol. 22*, 191−214.
34. Shaw, G., and Bell, J. N. B. (1994) *Plants and Radionuclides.* in *Plants and the Chemical Elements* (Farago, M. E., Ed.) VCH, Weinheim and New York.

BI990023U